One-Component Nanocomposite Membranes from Polymer Grafted Cellulose Nanocrystals

Harrison R. Paul¹, Matthew V. Tirrell*, 1,3 and Stuart J. Rowan*,1,2,4

¹ Pritzker School of Molecular Engineering, University of Chicago, Chicago, IL 60637, USA

² Department of Chemistry, University of Chicago, Chicago, IL 60637, USA

³ Materials Science Division and Center for Molecular Engineering, Argonne National Laboratory, 9700 S. Cass Ave., Lemont, IL 60434, USA

⁴ Chemical Science and Engineering Division and Center for Molecular Engineering, Argonne National Laboratory, 9700 S. Cass Ave., Lemont, IL 60434, USA

^{*}Email Addresses for Corresponding Authors: stuartrowan@uchicago.edu and mtirrell@uchicago.edu

Abstract

Membrane filtration is an important industrial purification process used to access clean, potable water. The fabrication of the membranes used in these purification applications often involves expensive and energy intensive processes that have a large negative impact on the environment. Sustainable alternatives with high water flux and strong rejection performance are needed to purify water. The focus of this work was to investigate the use of polymer grafted cellulose nanocrystals (CNCs) in membrane applications. The impact of the polymer grafting density and polymer conformation was investigated and showed that by increasing the grafting density of PEG such that it adopted a semi-dilute polymer brush conformation, the water flux through the membranes could be increased from 3.5 L hr⁻¹ m⁻² to 2900 L hr⁻¹ m⁻² for CNC membranes without and with grafted PEG, respectively. These membranes also exhibited rejection performances with molecular weight cut-offs between 62 kDa and 100 kDa for all polymer grafted samples, consistent with the ultrafiltration regime. Thus, the design of these one-component composite materials can enhance the water permeability of ultrafiltration membranes while maintaining effective selectivity.

KEYWORDS: Cellulose Nanocrystals, Polymer Grafted Nanoparticles, Water Transport, Membrane Filtration, Polymer Brush

Introduction

As the global demand for water from industrial processes, agriculture, and personal consumption increases, natural reservoirs are becoming progressively more strained. The regions that rely on these strained reservoirs are in turn becoming water-stressed, such that their demand for water has, or soon will, exceed the availability of the resource. The stress on these limited clean water resources is heightened by increased urbanization, coupled with industrial expansion across these

water-stressed regions.^{1,2} As the supply of clean water is decreasing, there is a significant increase in the need for potable water to be produced from underutilized sources, like contaminated fresh water and wastewater. Based on reports from the US Environmental Protection Agency (EPA), only 7 to 8% of the thirty-two billion gallons of waste effluent produced each day are recycled.³ To help address these issues, several technologies like membrane filtration,^{4–7} flocculation,^{8,9} and sorbents^{10,11} are used to generate potable water.

One of the most common methods of water purification is membrane filtration, as it typically exhibits a sufficiently high separation efficiency to provide high quality water with low chemical sludge effluent.⁴ Membrane filtration is a process that separates molecules of different sizes and characteristics through the use of a pressure differential to drive separation through a specific membrane. One class of membranes, namely porous films, rely on size exclusion, which depends on the membrane's microstructure, or adsorption, and can target specific solutes based on the surface chemistry of the membrane to separate contaminants from water.^{4,7,12} Filtration membranes are classified into different regimes based on their pore sizes, i.e. microfiltration (5 to 0.1 µm), ultrafiltration (0.1 to 0.01 μm), nanofiltration (0.01 to 0.001 μm), or reverse osmosis membranes (0.001 to 0.0001 µm or nonporous).^{4,13} These pore sizes in turn determine the types of contaminants that each membrane can remove. For example, ultrafiltration membranes are suitable for the removal of bio-based contaminants such as viruses or proteins from water. ¹³ However, there are several challenges that must be resolved in order for membrane filtration technology to fully meet the growing demand for potable water. Some of these challenges include improved water permeability, membrane stability, environmental impact, fouling, and water solute selectivity.^{4,14}

Typical materials used for ultrafiltration membranes include inorganic ceramics, ¹⁵ as well as organic polymers like polyacrylonitrile (PAN), ¹⁶ polysulfone amides (PSA), ⁴ polysulfone

(PSU),¹⁷ polyether sulfone (PES),¹⁸ and polyvinylidene fluoride (PVDF).^{4,12,19} Many of these membrane materials are produced using chemicals from petroleum-based sources, often requiring a significant number of organic solvents and small molecule components to manufacture functional membranes.^{20,21}

Natural biopolymers derived from low-cost, renewable bio-sources such as algae, plants, and microbes represent promising foundations for sustainable membrane alternatives that are petroleum-free and can be fabricated and modified in aqueous solutions instead of organic solvents.^{22,23} In particular, various polysaccharides including chitosan^{24–26} and cellulose^{27–31} have been utilized in water purification applications.²² Cellulose is a particularly promising material, as it is the most common biopolymer on the planet with a surface that can be engineered through facile chemical modification to introduce functional moieties.^{32–34} In fact cellulose derivatives, such a cellulose acetate, 35,36 are commonly used as membrane materials. However, they are chemically modified and fabricated into membranes using processes that requires large amounts of organic solvents and produces a significant amount of waste. 37,38 Nanocelluloses, such as cellulose nanofiber (CNFs) and cellulose nanocrystals (CNCs), have also recently received some attention as membrane materials. CNCs are highly crystalline, rod-like nanoparticles that can be isolated from a variety of different bio-sources, like cotton, wood, or fast-growing grasses such as Miscanthus x. Giganteus (MxG). 23,39-41 CNCs make promising candidates for membrane applications on account of their mechanical strength, chemical stability, and hydrophilic surface chemistry. Their high mechanical strength is a potential advantage if the material needs to withstand the high-pressure conditions required for ultrafiltration as well as nanofiltration, ⁴² while their inherent hydrophilicity is an advantage to reduce the fouling of the membrane surface.⁴³

Nanocellulose can be used to enhance the water permeability and anti-fouling properties of membranes by blending them into the polymer matrix and using that two-component nanocomposite as a barrier layer. 44,45 Additional studies have investigated the potential of nanocellulose as the sole component of the membrane barrier layer. Many of these membranes were designed to be affinity membranes focusing on the removal of charged contaminants like metal ions or organic dyes from solution via adsorption. 42,46 However, Mautner *et al.* has shown that size exclusion based ultrafiltration membranes can be fabricated from nanocellulose without being blended with a polymer. While these membranes exhibited flowrates comparable to commercially available membranes, the barrier layers were prone to point defects that could compromise the selectivity of the membranes. Additionally, the pore sizes were shown to be dependent on the dimensions of the nanocellulose used in the fabrication of the membrane with larger diameter nanoparticles leading to larger pore sizes; therefore, the selectivity of these nanocellulose barrier layers is limited and these materials cannot be easily tuned to target specific contaminants.

Thus, the goal of this work is to explore if grafting polymers with different molecular weights and grafting densities to the CNCs can be used to tailor their performance in membrane applications. Polymer-grafted CNCs can be processed directly into what has been termed a one-component nanocomposite (OCNs) film.^{47–49} The covalently linked nature of these materials prevents phase separation between the nanofiller and the polymer and as such allows access to a wider range of polymer to nanofiller ratios than traditional two-component composites.⁴⁹ Prior work on OCNs of polymer grafted CNCs has shown that such materials exhibit enhanced toughness and, in some cases, enhanced ion transport over equivalent two-component composites.^{49–51} Thus, it was of interest to see how functionalization of the nanocellulose with a

polymer impacted the behavior of the resulting OCN membranes. As such, reported herein is the exploration of poly(ethylene glycol) (PEG) grafted CNCs as the OCN barrier layer for ultrafiltration membranes (Figure 1). A specific focus of this work is to explore how polymer graft

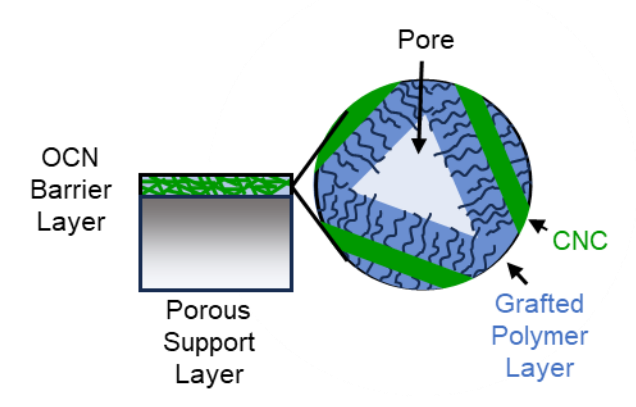


Figure 1. Schematic illustration of polymer grafted CNC membranes. The anisotropic thin-film composite membranes are composed of a one-component nanocomposite barrier layer on top of a porous membrane support structure. The OCN barrier layer is composed of distinct polymer grafted CNCs with pores in between the outer edges of their tethered polymer regions.

molecular weight and density impacts the properties of these membranes.

Experimental Section

Materials

Miscanthus x. Giganteus (MxG) pulp was provided by Aloterra Energy, LLC. Sodium hydroxide (NaOH), sodium hypochlorite (NaOCl), acetic acid, dimethylformamide (DMF) potassium cyanide (KCN), ninhydrin, butanol, and phenol were purchased from Thermo Fisher Scientific. Sodium chlorite (NaClO₂), hydrochloric acid (HCl), 2,2,6,6-tetramethylpiperidine 1-oxyl (TEMPO), sodium bromide (NaBr), and N-hydroxysuccinimide (NHS) were purchased from Millipore Sigma. 1-Ethyl-3-(3-dimethylaminopropyl) carbodiimide (EDC) was purchased from Combi-Blocks. Amine-terminated methoxy poly(ethylene glycol) (PEG-NH2) of various molecular weights (750, 5k, 10k g mol-1) were purchased from CreativePEGWorks. All water used was deionized in-house and all chemicals were used as-received without further purification.

Cellulose Nanocrystal Isolation from *Miscanthus x. Giganteus*

Preparation of the MxG-CNC-COOH

Ground *MxG* stalks (266.6 g) were soaked in 4 L of 2 wt% sodium hydroxide solution at room temperature for 24 hrs. The stalks were then treated twice more with 4 L 2 wt.% sodium hydroxide solutions at 95°C for 24 hours each. After each treatment, the stalks were washed with deionized (DI) water until the permeate was neutral pH. The pulp was then suspended in 4 L of 2 wt.% sodium chlorite solution and 15 mL of glacial acetic acid and heated to 70°C for 2 hrs. After the reaction, the solution was vacuum filtered and washed with DI water until the solid was white with no other color. To isolate the CNCs, hydrolysis was carried out by suspending the bleached white pulp in 4L of 1M HCl. This slurry was then heated to 75°C and stirred for 15 hrs. The mixture was then cooled at room temperature before being vacuum filtered and rinsed with DI water until the permeate was neutral. The solids were then subjected to dialysis with DI water for 5 days with the external solution being replaced twice every day. The solutions were freeze-dried to obtain the alcohol functionalized *MxG* CNCs (*MxG*-CNC-OH) as a white crystalline solid. *Synthesis of MxG*-CNC-COOH from *MxG*-CNC-OH via TEMPO oxidation

In order to synthesize the MxG-CNC-COOH samples, TEMPO oxidation was conducted following the previously published procedure with slight modifications. ^{23,52} 21.6 g of MxG-CNC-OH were dispersed into 1500 mL of DI water. Simultaneously, 1.7 g of TEMPO, 16.9 g of NaBr, and 138 g of NaOCl were dissolved into 500 mL of DI water. These two solutions were then mixed together and the pH was adjusted to 10 with NaOH and HCl. Once at pH 10, the reaction was allowed to proceed for 4.5 hrs with the pH being checked every half hour. The reaction was then quenched with 40 g of sodium chloride before being filtered and washed with DI water. The solid

was redispersed in DI water and dialyzed for 5 days before being freeze-dried to produce *MxG*-CNC-COOH.

*Grafting PEG-NH*² *to MxG-CNC-COOH*

MxG-CNC-COOH were suspended in DI water at 10 mg mL⁻¹ using a sonic bath to promote dispersion. Relative to the carboxylate content determined by conductivity titration, PEG-NH₂ (1 eq.) of the desired molecular weight was added to the CNC suspension and allowed to dissolve. EDC (3 eq.) was added and stirred for 15 min before adding NHS (3 eq.). The reaction proceeded overnight before centrifuging and resuspending in DI water. This new CNC suspension was dialyzed in dialysis tubing with a 10k MWCO to remove any remaining EDC, NHS, and free polymer. The PEG grafted CNC (MxG-CNC-g-PEG) suspension was dialyzed until a Kaiser test for primary amines confirmed that the free polymer had been removed. To perform the Kaiser test, three separate solutions were prepared for the testing process: (A) KCN (0.65 mg) was dissolved in DI water (1 ml) then added to pyridine (49 ml), (B) ninhydrin (1 g) was dissolved in butanol (20 ml), and (C) phenol (40 g) was dissolved in butanol (20 ml). To conduct a test, sample solution (1 ml) was placed in a vial on a hot plate at 100°C. Two drops of each solution were added and allowed to react, shaking occasionally. The color of the test solution was then compared to a control solution that had no primary amines. Once the test sample did exhibit a color change the MxG-CNC-g-PEG suspension was deemed to no longer contain a significant amount of free polymer. After purification, the resulting MxG-CNC-g-PEGs were suspended in water and freeze dried to obtain a fluffy white powder. To access samples with various grafting density, this process was repeated with varying amounts of PEG-NH₃ (0.5 eq., 1.5 eq., and 2 eq. for MxG-CNC-g-PEG_{5k} 0.02, MxG-CNC-g-PEG_{5k} 0.07, and MxG-CNC-g-PEG_{5k} 0.10, respectively).

Preparation of MxG-CNC-g-PEG Membranes

To prepare *MxG*-CNC-*g*-PEG membranes, 100 mg of each sample was suspending in deionized water at a concentration of 1 mg mL⁻¹. These suspensions were then vacuum filtered onto cellulose filter paper with an average pore size of 0.2 μm. The filtrate was then collected and passed through the membrane twice more to ensure that any CNCs that passed through the filter were collected. The membranes were then dried under ambient conditions overnight.

Conductivity Titration

The functional group density of the *MxG*-CNC-COOH samples was determined by conductometric titration. 75 mg of the *MxG*-CNC-COOH were dispersed into 150 mL of DI water using sonication. 15 µL of 12 M hydrochloric acid was added to 50 mL of the CNC dispersion to lower the solution's pH to 2-3. This suspension was then titrated with 0.01 M sodium hydroxide. In order to determine the charge density on the surface of the CNCs, the volume of 0.01 M sodium hydroxide used to titrate the weak acid functional groups in the conductometric titration was determined in Figure S1. The length of the initial trend line represents the volume of 0.01 M NaOH used to titrate the strong acid functional groups, while the plateau region corresponds to the weak acid functional groups. From the volume of NaOH used to titrate these functional groups, the functional group density on the CNC surface can be determined by:

Functional Group Density =
$$\frac{CV_{NaOH}}{M}$$

Where C is the concentration of NaOH, V_{NaOH} is the volume of NaOH used to titrate the functional groups based on the difference between where the trendlines intersect, and M is the mass of CNCs in kg.

Degree of Crystallinity

Wide angle X-ray scattering (WAXS) conducted at the 12-ID-B beamline at the Advanced Photon Source at Argonne National Laboratory was used to determine the degree of crystallinity of the CNCs after hydrolysis and oxidation. The CNCs were packed tightly into a washer and held in place between two pieces of Kapton tape. The data was then processed using the SAXS GUI software at the beamline before being analyzed with the SAS Irena package in IGOR Pro 7. The crystallinity index of the samples was determined with the peak deconvolution method with a Gaussian fit.

Thermogravimetric Analysis

The total amount of PEG in the MxG-CNC-g-PEG samples was measured using high resolution thermogravimetric analysis (Hi-Res TGA). The Hi-Res TGA procedure slows the heating rate when a mass loss event is detected so that the distinction between degradation events for cellulose degradation and PEG degradation can be improved. For these samples, procedure was conducted with the default settings (sensitivity = 1, amplitude 5 °C, period 200 s, ramp = 5 °C min⁻¹ to 600°C, resolution = 6) in platinum pans. Taking the derivative of the mass loss curve and fitting with multipeak fitting software, the area under the peak associated with PEG degradation can be measured to determine the weight fraction of PEG relative to CNC. Based on this analysis, a polymer grafting density can be obtained. The calculations for these conversions can be found in the Supporting Information.

Atomic Force Microscopy

Atomic force microscopy (AFM) was conducted on a Cipher ES Environmental AFM. Samples were prepared on a freshly-cleaved mica surface by first drop-casting poly(L-lysine), gently rinsing with DI water, then drop-casting the desired CNC sample suspended in DI water at

0.005 wt.%. The solution was allowed to sit for 3 minutes before once again gently rinsing with DI water before drying overnight. The samples were imaged in tapping mode with FS-1500 probes from Asylum Research and data was analyzed with Gwyddion software (Czech Metrology Institute).

Tensile Testing

Tensile testing was performed on each sample using a Zwick-Roell zwickiLine Z0.5 materials testing instrument. 5 mm wide strips were cut from each sample and strained at room temperature at a rate of 1 mm per min until break. Each membrane was tested in triplicate.

Scanning Electron Microscopy

SEM images of the cast membranes were taken with a Carl Zeiss Merlin high-resolution Field Emission Scanning Electron Microscope (FE-SEM). The SEM was operated under the In-Lens mode with an acceleration voltage of 1.0 kV with a working distance of 2–3 mm. The samples were placed on copper tape stuck onto stubs, and sputter-coated with with a thin layer (~4 nm) of Pt/Pd alloy using a Cressington 108 Auto Sputter Coater to reduce electron beam charging and improve the image quality.

Dead-end Filtration Flux Tests

To prepare samples for flux measurements, 25 mm disks were punched out of each *MxG*-CNC-*g*-PEG membrane. These membrane samples were then placed at the base of an Amicon Stirred Cell, which was then filled with 10 mL of DI water. As such the duration of each experiment varied depending on the water flux through each sample membrane. The stirred cell was connected to a nitrogen tank and pressurized to 2 bar. The permeate was collected in a beaker on a mass balance that was connected to computer so that the mass flowrate through each membrane could be measured over time (Figure S2).

Molecular Weight Cut-Off Measurements

To determine the rejection performance of each membrane, the same experimental set up from the flux tests was used except the DI water was replaced with polymer solutions. These polymer solutions were prepared by dissolving PEG with molecular weights of 10 kDa, 35 kDa, and 100 kDa into DI water at a concentration of 5 mg mL⁻¹. These solutions were then flowed through each membrane, and the permeates were collected. In order to mitigate fouling, the solution was stirred for the duration of the test, and the membranes were washed between trials. Two mL of each permeate was then freeze dried before being resuspended in 2 mL of DMF. The concentration of these solutions was then determined by RI detection in a DMF gel permeation chromatography instrument.

Helium Pycnometer Density Measurements

The volume of each MxG-CNC membrane was measured with an Anton-Paar Ultrapyc 5000. In order to calculate density, each sample was weighed before being placed in the sample chamber of the pycnometer. Each sample was placed into the microcell with filler metal spheres to reduce the void space of the cell and increase the accuracy of the measurements. The cell was pressurized to 18 psi with helium at 25 °C for each test. Each measurement was repeated 8 times.

Results and Discussion

Isolation and Functionalization of Cellulose Nanocrystals

Miscanthus x. Giganteus (MxG) is the biosource used access the cellulose nanocrystals and the MxG-CNC-COOH's were obtained from this biosource according to established literature procedures.^{23,52} The MxG stalks undergo mechanical processing, base washes, and acid washes to isolate the CNCs. Carboxylate groups are then introduced to the surface of the CNCs through (2,2,6,6-tetramethylpiperidin-1-yl)oxyl (TEMPO)-mediated oxidation in aqueous dispersions

(Figure 2(a)). These carboxylate groups serve to improve the dispersion of the CNCs in solution as the electrostatic repulsion mitigates CNC aggregation, while also providing a reactive moiety for further functionalization. The density of carboxylates on the CNC surface was determined (via conductivity titration) to be ca. 1000 mmol/kg, which is equivalent to ca. 1.14 carboxylate groups per nm² (Figure S1). The MxG-CNC-COOH exhibited a crystallinity index of 0.85 as measured by wide angle X-ray scattering (Figure S3) and the dimensions of the crystals (determined by AFM with a n=10 for all measurements) had an average length of 300 ± 120 nm, a width of 8.5 ± 2 nm, and a height of 3.3 ± 0.7 nm (Figure 2(b)).

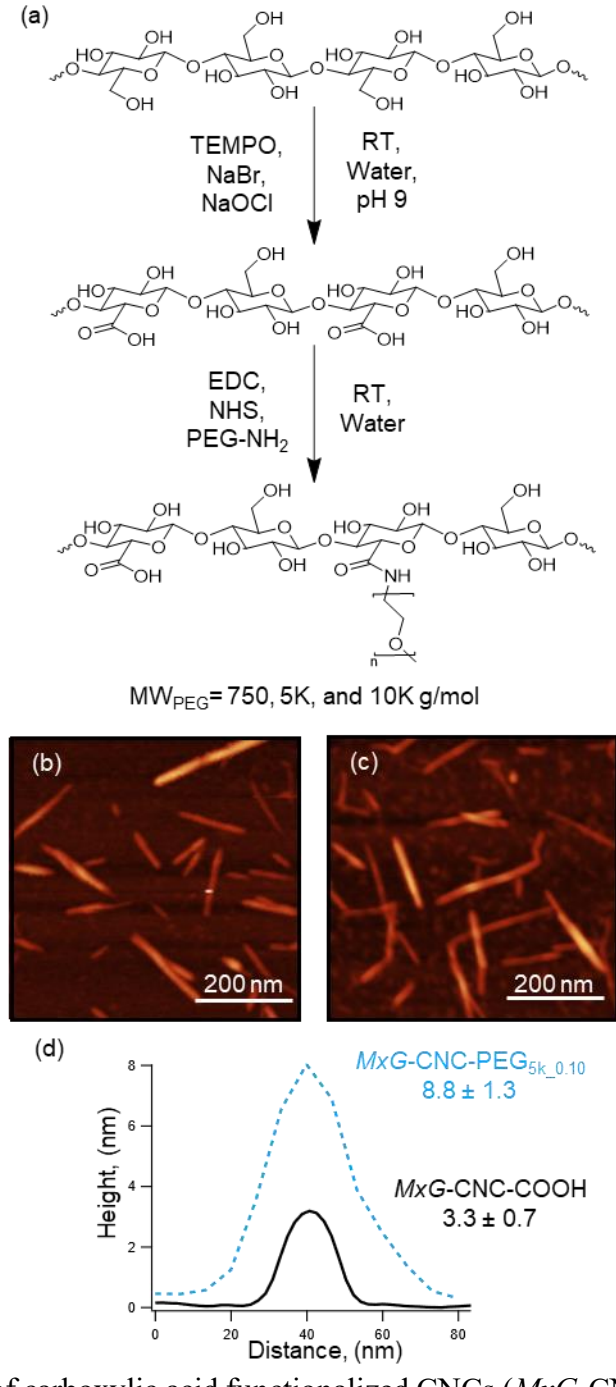


Figure 2. (a) Synthesis of carboxylic acid functionalized CNCs (*MxG*-CNC-COOH) followed by the subsequent grafting reaction to attach PEG-NH₂ to the CNCs, (b) AFM height image of *MxG*-CNC-COOH, (c) AFM height image of *MxG*-CNC-g-PEG_{5k_0.10} (PEG_{5k_0.10} refers to 5000 g mol⁻¹ grafted using EDC/NHS at a grafting density of 0.10 chains per nm²), and (d) a representative AFM height profile comparison for an average of 10 measurements between *MxG*-CNC-COOH and *MxG*-CNC-g-PEG_{5k_0.10}

Amine-terminated methoxy poly(ethylene glycol) (PEG-NH₂) of various molecular weights, 750 g mol⁻¹, 5k g mol⁻¹, and 10k g mol⁻¹, was grafted to the MxG-CNC-COOH (Figure 2(a)) using 1ethyl-3-(3-dimethylaminopropyl) carbodiimide (EDC) and N-hydroxysuccinimide (NHS) as coupling agents in deionized water following literature procedures. 52,53 The resulting polymer grafted CNCs (termed MxG-CNC-g-PEGx, where x is represents the M.Wt. of the PEG graft in g/mol, 750, 5k, or 10k) exhibit an increase in height from 3.3 ± 0.7 nm to 8.8 ± 1.3 nm after grafting for MxG-CNC-g-PEG_{5k}, which is consistent with successful covalent attachment of the PEG-NH₂ to the CNC surface (Figure 2(c) and 2(d)). 49,52 It is worthy of note that the measured increase in height takes into account the addition of grafted polymer to both the top and bottom surface of the CNC such that the height of each PEG brush is approximately half of the measured increased height. MxG-CNC-g-PEG_{10k} also exhibits an increase in height to 5.0 ± 0.2 nm, while the MxG-CNC-g-PEG₇₅₀ shows only a slight change in height $(4.2 \pm 0.5 \text{ nm})$ relative to the height of the ungrafted MxG-CNC-COOH (Figure S3). The change in height of the grafted polymer is related to both the molecular weight and density of the grafted polymer (vide infra) - higher grafting density leads to a more extended polymer conformation and as such larger particles.

To determine the amount of PEG grafted to the CNCs high-resolution thermogravimetric analysis (Hi-Res TGA) was used. The degradation of the *MxG*-CNC-g-PEG samples exhibit three degradation events as observed in the Hi-Res TGA data (a-c in Figure 3 and Figure S5). Based on the TGA of the MxG-CNC-COOH and the PEG-NH₂ the lower temperature degradation events (a and b) are associated with cellulose degradation, while the higher temperature degradation event (c) corresponds to PEG degradation. To estimate the weight fraction of PEG in these samples, a peak deconvolution method with a Lorenztian fit was used to determine the contribution of each

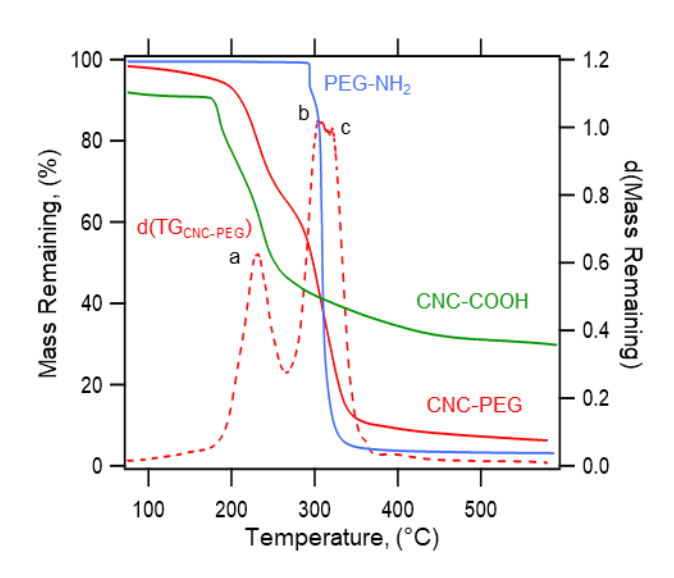


Figure 3. Hi-Res TGA curves of MxG-CNC-COOH (green), PEG-NH₂ (blue), and MxG-CNC-g-PEG_{5k_0.10} (solid red). The derivative of MxG-CNC-g-PEG_{5k_0.10} is presented to highlight the degradation events corresponding to cellulose (labeled a and b) and PEG degradation (labeled c).

Table 1. Polymer content and grafting density for MxG-CNC-g-PEG samples with various

molecular weights of grafted PEG.

	Grafted Polymer	Polymer Volume Fraction	Grafting Density
Sample	(wt%)	(%)	(Chains/nm ²)
MxG-CNC-g-PEG ₇₅₀	14	18	0.25
MxG -CNC- g -PEG _{5k_0.02}	8	10	0.02
MxG -CNC- g -PEG _{5k_0.05}	17	21	0.05
MxG -CNC- g -PEG5 k_0 0.07	24	30	0.07
MxG-CNC-g-PEG5k_0.10	31	37	0.10
<i>MxG</i> -CNC- <i>g</i> -PEG _{10k}	32	38	0.05

component to the peaks of the dTG curve (Figure S6). The area under these fits were integrated to estimate PEG weight fractions, which ranged from 8 to 32 wt.% (Table 1) depending on the sample, which corresponds to volume fractions from 10 to 38% PEG (Table 1, Section S1). The weight fractions were used to calculate the grafting density of each sample, which ranges from

weight fractions were used to calculate the grafting density of each sample, which ranges from 0.02 to 0.25 chains per nm² (Table 1, SI Section S2).⁵²

It has been shown in the polymer brush literature on planar surfaces that molecular weight and grafting density each play a role in the nature of the polymer conformation of the grafted brush.⁵⁴ In order to explore if the grafted polymer conformation plays a role in the resulting properties of the PEG grafted CNC membranes, in addition to varying the molecular weight of the grafted PEG, the MxG-CNC-g-PEG_{5k} material was prepared at different grafting densities. The initially synthesized MxG-CNC-g-PEG_{5k} has a grafting density of 0.10 chains/nm². To access samples with different grafting densities, the same grafting procedure was performed with varying equivalents of PEG-NH₂ from 0.5 eq. to 2 eq. The different MxG-CNC-g-PEG_{5k} samples were then purified with dialysis until amine-sensing Kaiser tests confirmed the absence of unreacted PEG-NH₂.55 The resulting samples are labeled MxG-CNC-g-PEG_{5k} y, where the y indicates their relative grafting densities in chains/nm², 0.02, 0.05, 0.07, and 0.10, (Table 1). As one might expect the height of the grafted CNCs as obtained by AFM decreases with grafting density going from 8.8 ± 1.3 nm, 5.5 ± 0.5 nm, 4.3 ± 0.1 nm to 3.7 ± 0.2 nm for the MxG-CNC-COOH_{5k} y where y=0.1, 0.07, 0.05 and 0.02, respectively. The lower grafting density sample MxG-CNC-COOH_{5k} 0.02 has a height of that is statistically equivalent to the height of MxG-CNC-COOH (Figure S4).

The tethered polymer conformations can be divided into three regimes, namely the mushroom regime, the semi-dilute brush regime (SDPB), and the concentrated brush regime (CPB). 49,54,56–58 The radius of gyration (Rg) and the grafting density of the tethered polymer largely influence which conformation will be adopted by the grafted polymer. 48 The mushroom regime is defined by the phase space in which the tethered polymers are spread across the surface such that adjacent chains do no interact with each other. 49,52 As such, the boundary of mushroom regime is the point at which

each polymer chain's conformation would be influenced by its neighbors for a given molecular weight. As grafting density is increased to the point that neighboring chains are at a distance less than R_g from each other, the polymers adopt a SDPB conformation.⁵⁹ In this regime, the polymers extend away from the nanoparticle surface and deviate from the loose coil conformation seen in the mushroom regime. As chains are packed more densely on the nanoparticle surface, the polymers enter the CPB regime, where they elongate to form a stiffer polymer layer. For polymer grafted nanoparticles that exhibit a CPB, the polymer chains with sufficiently high molecular weights may transition from a CPB to a SDPB regime at some radial distance away from the particle's surface on account of the innate curvature of the nanoparticle causing 86 the volume to increase in accordance with predictions by Daoud-Cotton models applied to nanoparticles. 49,60-62 With the grafting densities calculated and the molecular weights known, it was possible to determine the nature of the grafted polymer conformations by plotting the grafting density and molecular weight of the grafted PEG onto a tethered polymer phase diagram (Figure 4). The transition between the mushroom and brush regimes (the red line in Figure 4) was defined by taking the inverse of the area of a circle defined by the R_g of the grafted polymer that would be projected onto the surface. 49,52,58 The concentrated brush to semi-dilute brush transition (the teal line in Figure 4) was calculated based on work by Hansoge et al. using their model of polybutadiene, which exhibits a similar persistence length to PEG.52,63 Based on this phase diagram, MxG-CNC-g-PEG₇₅₀, MxG-CNC-g-PEG_{5k_0.02}, and MxG-CNC-g-PEG_{5k_0.05} each appear to fall in the mushroom regime, while MxG-CNC-g-PEG_{5k_0.07}, MxG-CNC-g-PEG_{5k_0.10}, and MxG-CNC-g-PEG_{10k} have moved more into the semi-dilute polymer brush regime.

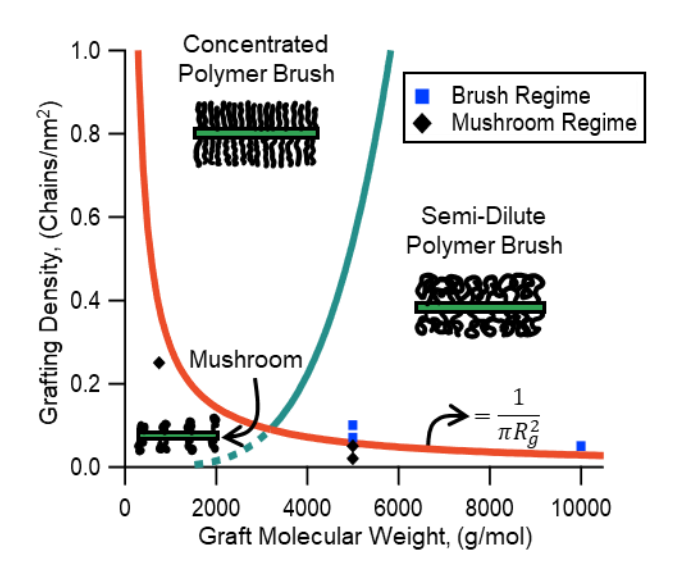


Figure 4. Polymer conformation phase space with synthesized MxG-CNC-g-PEG samples plotted. The concentrated polymer brush to semi-dilute polymer brush transition (teal line) is modeled based off polybutadiene.⁶³ The mushroom to brush transition (red line) is estimated based on the grafting density at which circles defined by the R_g of the polymer would start to overlap.

One-Component Nanocomposite Membranes

Membranes were prepared by vacuum casting the different MxG-CNC-g-PEG samples onto cellulose filter paper, with the MxG-CNC-g-PEG acting as the barrier layer and the cellulose filter paper providing additional support. This procedure was able to create mechanically robust membranes as demonstrated via tensile testing (Figure S7 and Table S1). As a control, MxG-CNC-COOH membrane samples were prepared using the same process. The morphologies of these membranes were characterized by scanning electron microscopy (SEM), which shows that the CNC nanoparticles appear to form porous, fibrous networks with individualized particles or bundles of nanoparticles visible in the images for MxG-CNC based membranes instead of a dense,

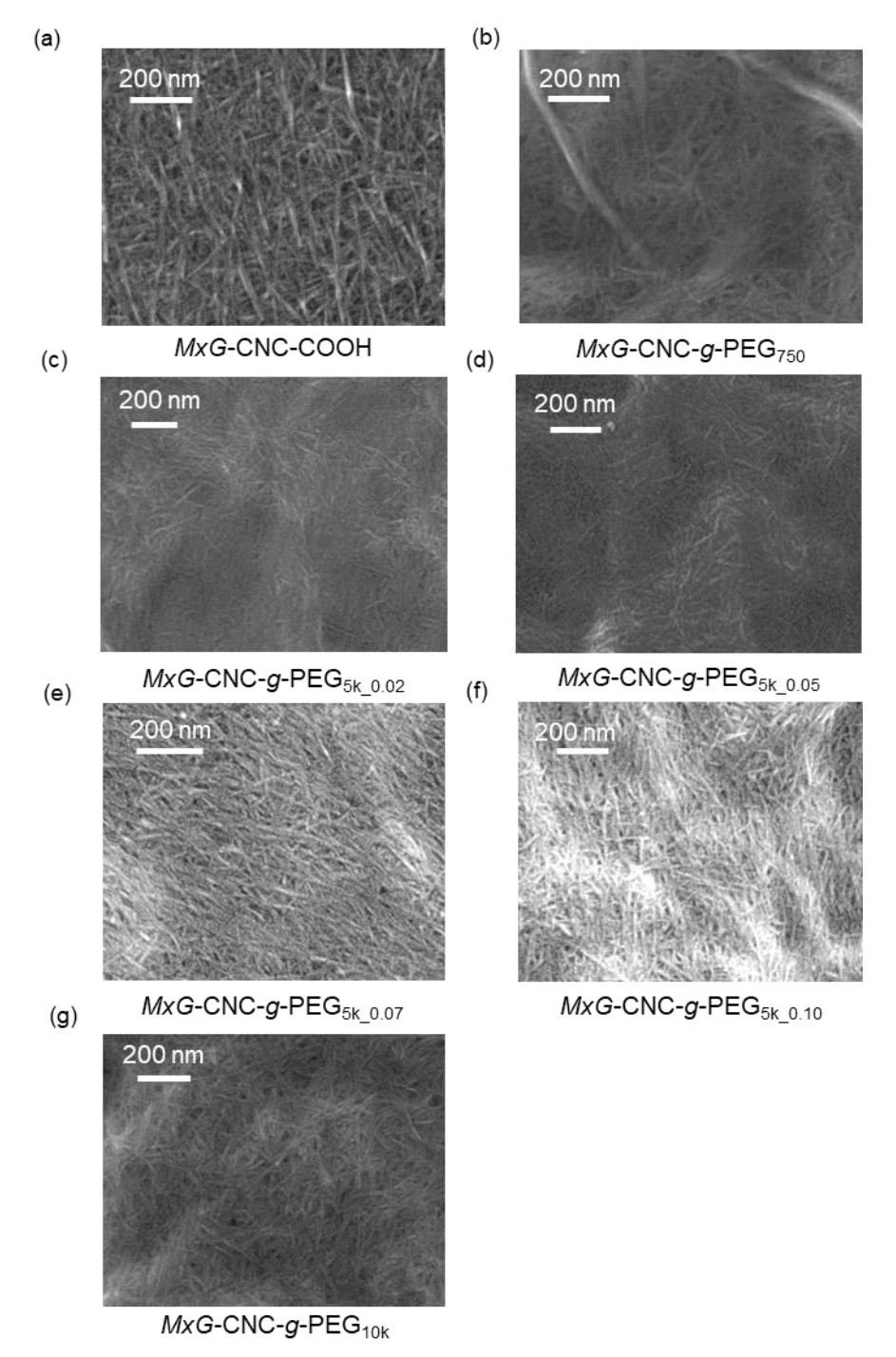


Figure 5. SEM images of MxG-CNC-COOH and MxG-CNC-g-PEG membrane surfaces with PEG of different molecule weights and grafting densities. (a) MxG-CNC-COOH, (b) MxG-CNC-g-PEG₇₅₀, (c) MxG-CNC-g-PEG_{5k_0.02}, (d) MxG-CNC-g-PEG_{5k_0.05}, (e) MxG-CNC-g-PEG_{5k_0.07}, (f) MxG-CNC-g-PEG_{5k_0.10}, (g) MxG-CNC-g-PEG_{10k}

solid polymer films (Figure 5). These membranes were tested in a dead-end filtration configuration to determine the flux of deionized water passing through the membranes under two bars of

pressure. The MxG-CNC-COOH membrane exhibits a water flux of $3.50 \pm 0.10 \, (\frac{L}{hr \, m^2})$ (Figure 6(a)). The samples in which the graft PEG is predicted to be in the mushroom regime, namely MxG-CNC-g-PEG₇₅₀ (3.27 \pm 0.71 ($\frac{L}{hr \, m^2}$)), MxG-CNC-g-PEG_{5k_0.02} (3.99 \pm 0.41 ($\frac{L}{hr \, m^2}$)), and MxG-CNC-g-PEG_{5k_0.05} 3.76 \pm 0.06 ($\frac{L}{hr \, m^2}$)), show no statistical improvement in the flux when compared to the MxG-CNC-COOH membranes (Figure 6(a) and 6(b)). This data also shows the polymer volume fraction in these samples, which ranges from 10% for MxG-CNC-g-PEG_{5k_0.02} to 21% for MxG-CNC-g-PEG_{5k} 0.05, has little-to-no effect on the flux through the membranes. However, the story appears different as the tethered polymer conformation transitions into the semi-dilute polymer brush regime. There is a significant increase in the water flux to 6.30 ± 0.05 g-PEG_{5k} 0.07, and the MxG-CNC-g-PEG_{5k} 0.10 samples, respectively (Figure 6(a) and 6(c)). It is worthy of note that the flux of 2900 ($\frac{L}{hr \, m^2}$) for MxG-CNC-g-PEG_{5k_0.10} is significantly higher than the flux of 6.30 $(\frac{L}{hr m^2})$ for MxG-CNC-g-PEG_{10k} even though these two samples have similar volume fractions of 37% and 38%, respectively, suggesting that the volume fraction of PEG in

Additional control experiments were conducted with blends of *MxG*-CNC-COOH and PEG-NH₂ to evaluate the role of covalent attachment between the PEG and the CNC nanoparticles. As might be expected these tests showed an increase in water flux after each additional test (not

these composites is not the only driver of the water flux through these materials.

observed in the *MxG*-CNC-*g*-PEG-based membranes) as the free PEG was washed through the membrane (Figure S8).

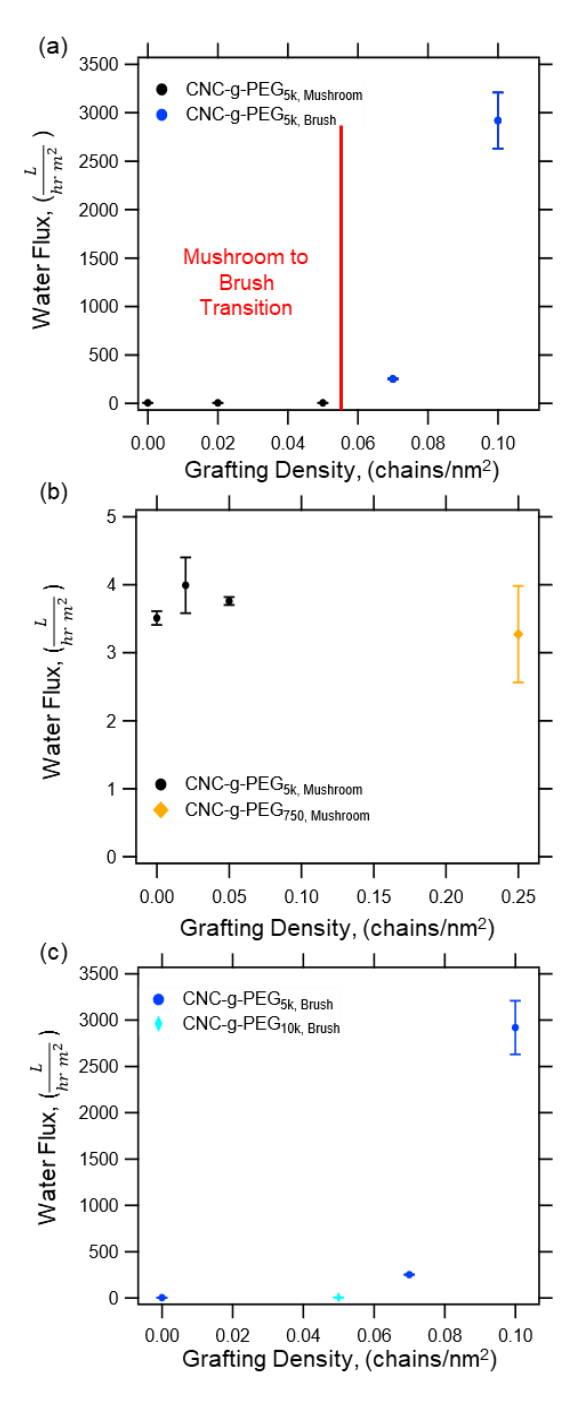


Figure 6. (a) Water flux for the MxG-CNC-g-PEG_{5k_y} samples as grafting density is increased from the mushroom regime (black circles) to the semi-dilute polymer brush regime (blue circles) with the transition point denoted with a solid red line. (b) Water flux of all mushroom regime samples as grafting density increases. (c) Water flux of all semi-dilute polymer brush samples as grafting density increases.

In addition to measuring the deionized water flux through these composite membranes, rejection performance of each membrane was evaluated by determining the molecular weight cut-off (MWCO) of each sample. The MWCO is defined as the molecular weight at which 90% of a tested solute is rejected and kept in the retentate and 10% of the solute with that particular molecular weight passing into the permeate. 4,29,64 For these studies, aqueous solutions of PEG polymers with molecular weights ranging from 10 kDa to 100 kDa with concentrations of 5 mg per mL were used as the solute to test the rejection performance of each membrane. The selectivity of the membranes was estimated by interpolating between the rejection percentages for PEG solutes with molecular weights of 35 kDa and 100 kDa for each sample (Figure 7(a)). The selectivity of the membranes with mushroom regime samples was shown to be 62 kDa for MxG-CNC-g-PEG₇₅₀, 100 kDa for MxG-CNC-g-PEG_{5k} 0.02 and 97 kDa for MxG-CNC-g-PEG_{5k} 0.05. The selectivity of the membranes fabricated from the brush regime samples was determined to be 65 kDa for MxG-CNC-g-PEG_{5k} 0.07, 82 kDa for MxG-CNC-g-PEG_{5k} 0.10, and 85 kDa for MxG-CNC-g-PEG_{10k}. Each of these membranes exhibited a reduction in the MWCO relative to the MWCO of the MxG-CNC-COOH samples, which was > 100 kDa (the rejection percentage for 100 kDa solutes was below 90% so an exact MWCO could not be determined). The MWCO is maintained within the low end of the ultrafiltration regime, namely between 1 kDa and 1000 kDa for all samples (Figure 7(b), which could have applications for targets in wastewater treatment, water remediation, recovery of surfactants in industrial cleaning, food processing, and protein separation.⁴ These materials also compare favorably to some existing commercially available membranes poly(vinylidene fluoride) based V4 ultrafiltration membranes, which exhibits a MWCO of 70 kDa and a flux of 67 to 104 $(\frac{L}{hr \, m^2 bar})^{.65}$ The selectivity appears to be not significantly impacted by either the amount or the grafting density of the bound PEG polymer. The tethered polymer morphology also does not seem

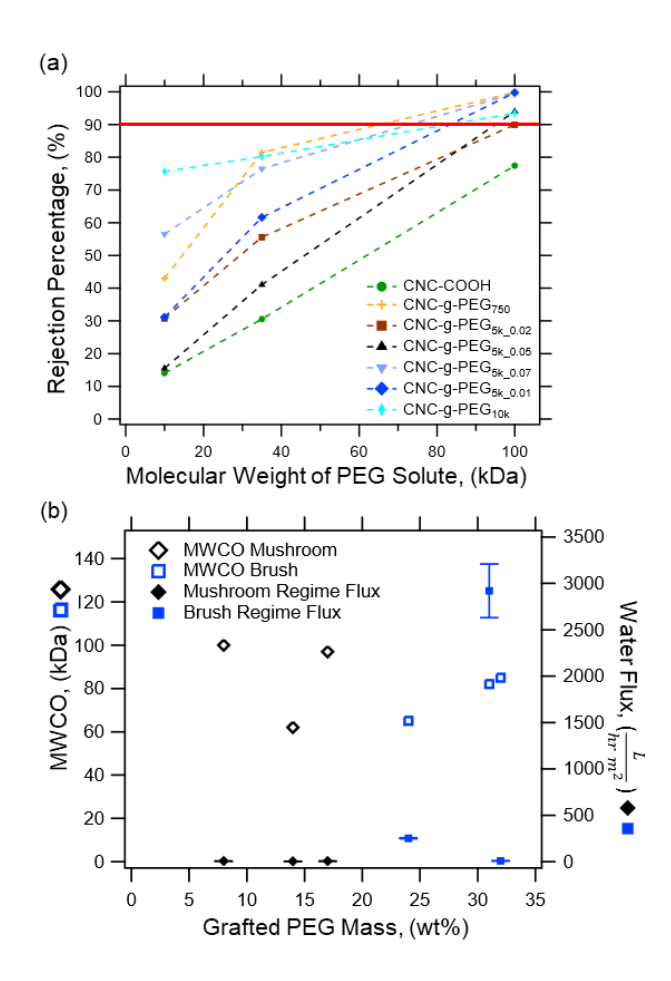


Figure 7. (a) The rejection of PEG is shown for MxG-CNC-COOH (green circles), MxG-CNC-g-PEG750 (orange plus symbols), MxG-CNC-g-PEG5k_0.02 (brown squares), MxG-CNC-g-PEG5k_0.05 (black up triangles), MxG-CNC-g-PEG5k_0.07 (periwinkle down triangles), MxG-CNC-g-PEG5k_0.10 (blue diamonds), and MxG-CNC-g-PEG10k (cyan thin rhomboids). The MWCO is the point at which 90% of the solute is rejected (red line). (b) The molecular weight cutoff (open diamonds for the mushroom regime samples and open squares for the brush regime samples) of MxG-CNC-COOH and MxG-CNC-g-PEG membranes and the water flux of the membranes with membrane regime samples denoted with black diamonds and the semi-dilute brush regime samples denoted with blue squares as a function of the amount of grafted polymer.

to change the selectivity of the membranes. This consistency may be expected for the samples in the mushroom conformation based on the previously observed flux trends for these materials. However, this result is perhaps a little surprising for the semi-dilute polymer brush regime samples since the water flux through these materials is drastically higher when compared to other samples, while the MWCO remains similar to the other grafted CNCs (Figure 7).

Based on literature precedent, MWCO data is commonly used to estimate pore size in ultrafiltration membranes using measured relationships between the MWCO and known pore size.⁴ According to these comparisons, the MWCO data indicate that the pore sizes within these materials remain on the order of a few nanometers.⁴ This pore size measured by MWCO likely correlates to the space between the polymer-grafted CNCs (labeled as "Pore" in Figure 1). The presence of these pores is consistent with the SEM images, which show that the MxG-CNC-g-PEG nanoparticles remain distinct from one another with spaces in between their cylindrical forms for each sample (Figure 5). Based on these flux data, the nature of the polymer brush on the samples can increase the rate of water transport through the membranes while maintaining similar pore sizes. As such, the structure of the membranes was evaluated with helium pycnometry to determine the density of these membranes as the polymer conformation shifted (Figure S10). These data show that the introduction of PEG to the surface of the CNCs leads to a reduction in the density of the samples. For example, MxG-CNC-COOH has a density of 1.71 ± 0.0004 g/(cm³) while the mushroom regime MxG-CNC-g-PEG₇₅₀ has a density of 1.61 \pm 0.0002 g/(cm³). A change in density is also observed with in the MxG-CNC-g-PEG_{5k} series. The density of the two mushroom regime samples is relatively constant at 1.62 ± 0.0002 g/(cm³) and 1.61 ± 0.0003 g/(cm³) for MxG-CNC-g-PEG_{5k} 0.02 and MxG-CNC-g-PEG_{5k} 0.05, respectively. However, a decrease in density is observed as the grafted PEG transitions into more into the brush regime with values of 1.58 \pm $0.0003 \text{ g/(cm}^3)$ for MxG-CNC-g-PEG_{5k_0.07} and $1.44 \pm 0.0003 \text{ g/(cm}^3)$ for MxG-CNC-g-PEG_{5k_0.10}. A similar low density $(1.53 \pm 0.0004 \text{ g/(cm}^3))$ is observed for the brush regime MxG-CNC-g-PEG_{10k}. Thus, the introduction of PEG brushes to the surface of the CNCs appears to shift how the nanoparticles pack together as the membrane is formed such that the structure is less dense, which correlates with the increased water flux.^{29,66,67}

While other studies have shown that controlling the degree of extension for a polymer brush in situ based on a salt response can restrict pore sizes and thus change the flux and selectivity of those membranes.⁶⁸ In this system, since the MWCO remains relatively constant, the average pore size does not appear to be changing significantly, so the introduction of the polymer brush may lead to an increase in the number of pores that are of similar sizes or potentially a reduction in tortuosity that leads to an increase in water permeability. It is also possible that the increase in flux for the brush regime *MxG*-CNC-*g*-PEG samples is aided, in part, by the PEG brushes increasing the water permeability of the membranes. For these brush samples, which are on the boundary of the mushroom to semi-dilute brush regimes, the PEG brush on the surface of the nanoparticle presumably remains water permeable, thus potentially increasing the effective radius of the pores to water,^{69–72} increasing the water flux. While the PEG brush on the surface of the nanoparticle should remain water permeable, the brush may sterically hinder transport of macromolecules through the membrane.^{69–71} This would then result in the water permeable volume of the membrane being larger than the effective pore size for macromolecules.

Irrespective of the exact mechanism, it is worth noting that for the materials in the CPB/SDPB regime, the flux increases with increasing grafting density. For these CPB/SDPB samples, higher grafting densities will lead to a larger fraction of CPB before the tethered polymer transitions to the SDPB phase. Based on the model from Hansoge et. al (Figure 4), the CPD/SDPB samples have CPB regime fractions of 27.5%, 60.0%, and 65.5% for MxG-CNC-g-PEG_{10k}, MxG-CNC-g-PEG_{5k_0.07}, and MxG-CNC-g-PEG_{5k_0.10}, respectively. As the flux through these samples is MxG-CNC-g-PEG_{10k} < MxG-CNC-g-PEG_{5k_0.07} < MxG-CNC-g-PEG_{5k_0.10}, this data suggests that the CPB regime may be more favorable to water transport than the SDPB. $^{70-72}$

Conclusions

A series of PEG grafted MxG-CNCs have been synthesized and membranes consisting of one-component nanocomposite barrier layers on top of cellulose-based support layers prepared. The water flux and selectivity of these composite MxG-CNC-g-PEG membranes were evaluated by stirred cell flux test and MWCO measurements. In particular, it was shown that the water flux through the membranes could be increased by orders of magnitude from 3.5 ($\frac{L}{hr m^2}$) to 2900 $(\frac{L}{hr m^2})$, while maintaining a MWCO under 100 kDa, through the addition of grafted PEG at a high enough grafting density such that the polymer graft adopted a CPB/SDB polymer conformation. This polymer-grafted CNC-based membrane appears (at least to some extent) to be able to decouple the traditional tradeoff between flux and selectivity. This system can also be synthesized and fabricated entirely in aqueous solutions removing the need for large volumes of organic solvents used to fabricate commercially available ultrafiltration membranes. This methodology could provide a modular platform for the design of higher-efficiency polymer grafted CNC membranes that are capable of selective removal or recovery of target contaminants by modifying the grafted polymers to include specialized functional groups. As such, studies of these materials' resilience under industrial membrane filtration conditions, exploring their long-term stability, antifouling properties, and chlorine resistance may be of interest. Additionally, studies of alternative grafting materials like phosphate binding proteins for the selective recovery of dissolved solids may also be of interest.

Supporting Information

Conductometric titration and WAXS of *MxG*-CNC-COOH samples, AFM and Hi-Res TGA of *MxG*-CNC-*g*-PEG samples, additional details of multipeak fitting for TGA of PEG grafted CNC samples, methods used to calculate volume fraction and grafting density of *MxG*-CNC-*g*-PEG samples, and water flowrate through non-grafted PEG CNC membranes.

Acknowledgements

This work was supported in part by National Science Foundation PIRE program under Grant No. NSF #1743475, the NSF Center for Sustainable Polymers (CSP) (CHE-1901635) at the University of Minnesota and by the Advanced Materials for Energy-Water Systems (AMEWS), an Energy Frontier Research Center funded by the U.S. Department of Energy, Office of Science, Basic Energy Sciences. It made use of the shared facilities at the University of Chicago Materials Research Science and Engineering Center (MRSEC), supported by National Science Foundation (NSF) under award number DMR-2011854. Parts of this work were carried out at the Soft Matter Characterization Facility of the University of Chicago. This research used resources of the Advanced Photon Source, a U.S. Department of Energy (DOE) Office of Science user facility operated for the DOE Office of Science by Argonne National Laboratory under Contract No. DE-AC02-06CH11357.

References

- (1) Vörösmarty, C. J.; Green, P.; Salisbury, J.; Lammers, R. B. Global Water Resources: Vulnerability from Climate Change and Population Growth. *Science* (1979) **2000**, 289 (5477), 284–288. https://doi.org/DOI: 10.1126/science.289.5477.284.
- Vörösmarty, C. J.; McIntyre, P. B.; Gessner, M. O.; Dudgeon, D.; Prusevich, A.; Green, P.; Glidden, S.; Bunn, S. E.; Sullivan, C. A.; Liermann, C. R.; Davies, P. M. Global Threats to Human Water Security and River Biodiversity. *Nature 2010 467:7315* **2010**, *467* (7315), 555–561. https://doi.org/10.1038/nature09440.
- (3) Epa, U.; Supply, W.; Resources Division, W.; Smith, C. 2012 Guidelines for Water Reuse. **2004**.
- (4) Lee, A.; Elam, J. W.; Darling, S. B. Membrane Materials for Water Purification: Design, Development, and Application. *Environ Sci (Camb)* **2016**, *2* (1), 17–42. https://doi.org/10.1039/C5EW00159E.
- (5) Hilal, N.; Al-Zoubi, H.; Darwish, N. A.; Mohamma, A. W.; Abu Arabi, M. A Comprehensive Review of Nanofiltration Membranes: Treatment, Pretreatment, Modelling,

- and Atomic Force Microscopy. *Desalination* **2004**, *170* (3), 281–308. https://doi.org/10.1016/j.desal.2004.01.007.
- (6) Klein, E. Affinity Membranes: A 10-Year Review. *J Memb Sci* **2000**, *179* (1–2), 1–27. https://doi.org/10.1016/S0376-7388(00)00514-7.
- (7) Baker, R. W. *Membrane Technology and Applications*; John Wiley & Sons, Ltd: Chichester, UK, 2012. https://doi.org/10.1002/9781118359686.
- (8) Fu, F.; Wang, Q. Removal of Heavy Metal Ions from Wastewaters: A Review. *J Environ Manage* **2011**, *92* (3), 407–418. https://doi.org/10.1016/J.JENVMAN.2010.11.011.
- (9) Liu, T.; Ding, E.; Xue, F. Polyacrylamide and Poly(N,N-Dimethylacrylamide) Grafted Cellulose Nanocrystals as Efficient Flocculants for Kaolin Suspension. *Int J Biol Macromol* **2017**, *103*, 1107–1112. https://doi.org/10.1016/J.IJBIOMAC.2017.05.098.
- (10) Crini, G. Non-Conventional Low-Cost Adsorbents for Dye Removal: A Review. *Bioresour Technol* **2006**, *97* (9), 1061–1085. https://doi.org/10.1016/J.BIORTECH.2005.05.001.
- (11) Crini, G.; Lichtfouse, E.; Wilson, L. D.; Morin-Crini, N. Conventional and Non-Conventional Adsorbents for Wastewater Treatment. *Environ Chem Lett* **2019**, *17* (1), 195–213. https://doi.org/10.1007/S10311-018-0786-8/.
- (12) Ulbricht, M. Advanced Functional Polymer Membranes. *Polymer (Guildf)* **2006**, *47* (7), 2217–2262. https://doi.org/10.1016/J.POLYMER.2006.01.084.
- (13) Jonsson, G. Molecular Weight Cut-off Curves for Ultrafiltration Membranes of Varying Pore Sizes. *Desalination* **1985**, *53* (1–3), 3–10. https://doi.org/10.1016/0011-9164(85)85048-7.
- (14) Werber, J. R.; Deshmukh, A.; Elimelech, M. The Critical Need for Increased Selectivity, Not Increased Water Permeability, for Desalination Membranes. *Environ Sci Technol Lett* **2016**, *3* (4), 112–120. https://doi.org/10.1021/acs.estlett.6b00050.
- (15) Kumar, S.; Ahlawat, W.; Bhanjana, G.; Heydarifard, S.; Nazhad, M. M.; Dilbaghi, N. Nanotechnology-Based Water Treatment Strategies. *J Nanosci Nanotechnol* **2014**, *14* (2), 1838–1858. https://doi.org/10.1166/JNN.2014.9050.
- (16) Lohokare, H. R.; Muthu, M. R.; Agarwal, G. P.; Kharul, U. K. Effective Arsenic Removal Using Polyacrylonitrile-Based Ultrafiltration (UF) Membrane. *J Memb Sci* **2008**, *320* (1–2), 159–166. https://doi.org/10.1016/J.MEMSCI.2008.03.068.
- (17) Saljoughi, E.; Mousavi, S. M. Preparation and Characterization of Novel Polysulfone Nanofiltration Membranes for Removal of Cadmium from Contaminated Water. *Sep Purif Technol* **2012**, *90*, 22–30. https://doi.org/10.1016/J.SEPPUR.2012.02.008.
- (18) Ahmad, A. L.; Abdulkarim, A. A.; Ooi, B. S.; Ismail, S. Recent Development in Additives Modifications of Polyethersulfone Membrane for Flux Enhancement. *Chemical Engineering Journal* **2013**, *223*, 246–267. https://doi.org/10.1016/J.CEJ.2013.02.130.

- (19) Liu, F.; Hashim, N. A.; Liu, Y.; Abed, M. R. M.; Li, K. Progress in the Production and Modification of PVDF Membranes. *J Memb Sci* **2011**, *375* (1–2), 1–27. https://doi.org/10.1016/J.MEMSCI.2011.03.014.
- (20) Lee, K. P.; Arnot, T. C.; Mattia, D. A Review of Reverse Osmosis Membrane Materials for Desalination—Development to Date and Future Potential. *J Memb Sci* **2011**, *370* (1–2), 1–22. https://doi.org/10.1016/J.MEMSCI.2010.12.036.
- (21) Soroko, I.; Bhole, Y.; Livingston, A. G. Green Chemistry Environmentally Friendly Route for the Preparation of Solvent Resistant Polyimide Nanofiltration Membranes. **2011**. https://doi.org/10.1039/c0gc00155d.
- (22) Nasrollahzadeh, M.; Sajjadi, M.; Iravani, S.; Varma, R. S. Starch, Cellulose, Pectin, Gum, Alginate, Chitin and Chitosan Derived (Nano)Materials for Sustainable Water Treatment: A Review. *Carbohydr Polym* **2021**, *251*, 116986. https://doi.org/10.1016/J.CARBPOL.2020.116986.
- (23) Cudjoe, E.; Hunsen, M.; Xue, Z.; Way, A. E.; Barrios, E.; Olson, R. A.; Hore, M. J. A.; Rowan, S. J. Miscanthus Giganteus: A Commercially Viable Sustainable Source of Cellulose Nanocrystals. *Carbohydr Polym* **2017**, *155*, 230–241. https://doi.org/10.1016/J.CARBPOL.2016.08.049.
- (24) Mende, M.; Schwarz, D.; Steinbach, C.; Boldt, R.; Schwarz, S. The Influence of Salt Anions on Heavy Metal Ion Adsorption on the Example of Nickel. *Materials* **2018**, *11* (3). https://doi.org/10.3390/MA11030373.
- (25) Khan, S. B.; Ali, F.; Kamal, T.; Anwar, Y.; Asiri, A. M.; Seo, J. CuO Embedded Chitosan Spheres as Antibacterial Adsorbent for Dyes. *Int J Biol Macromol* **2016**, *88*, 113–119. https://doi.org/10.1016/J.IJBIOMAC.2016.03.026.
- (26) Liu, J.; Chen, X.; Shao, Z.; Zhou, P. Preparation and Characterization of Chitosan/Cu(II) Affinity Membrane for Urea Adsorption. *J Appl Polym Sci* **2003**, *90*, 1108–1112.
- (27) Carpenter, A. W.; de Lannoy, C.-F.; Wiesner, M. R. Cellulose Nanomaterials in Water Treatment Technologies. *Environ Sci Technol* **2015**, *49* (9), 5277–5287. https://doi.org/10.1021/es506351r.
- (28) Jin, L.; Li, W.; Xu, Q.; Sun, Q. Amino-Functionalized Nanocrystalline Cellulose as an Adsorbent for Anionic Dyes. *Cellulose* **2015**, *22* (4). https://doi.org/10.1007/s10570-015-0649-4.
- (29) Mautner, A.; Lee, K.-Y.; Tammelin, T.; Mathew, A. P.; Nedoma, A. J.; Li, K.; Bismarck, A. Cellulose Nanopapers as Tight Aqueous Ultra-Filtration Membranes. *React Funct Polym* **2015**, *86*, 209–214. https://doi.org/10.1016/j.reactfunctpolym.2014.09.014.
- (30) Kamtsikakis, A.; McBride, S.; Zoppe, J. O.; Weder, C. Cellulose Nanofiber Nanocomposite Pervaporation Membranes for Ethanol Recovery. *ACS Appl Nano Mater* **2021**, *4* (1), 568–579. https://doi.org/10.1021/ACSANM.0C02881.

- (31) Köse, K.; Mavlan, M.; Youngblood, J. P. Applications and Impact of Nanocellulose Based Adsorbents. *Cellulose* **2020**, *27* (6), 2967–2990. https://doi.org/10.1007/S10570-020-03011-1.
- (32) Voisin, H.; Bergström, L.; Liu, P.; Mathew, A. P. Nanocellulose-Based Materials for Water Purification. *Nanomaterials (Basel)* **2017**, *7* (3). https://doi.org/10.3390/nano7030057.
- (33) Yu, X.; Tong, S.; Ge, M.; Wu, L.; Zuo, J.; Cao, C.; Song, W. Adsorption of Heavy Metal Ions from Aqueous Solution by Carboxylated Cellulose Nanocrystals. *Journal of Environmental Sciences* **2013**, *25* (5), 933–943. https://doi.org/10.1016/S1001-0742(12)60145-4.
- (34) Habibi, Y.; Lucia, L. A.; Rojas, O. J. Cellulose Nanocrystals: Chemistry, Self-Assembly, and Applications. *Chem Rev* **2010**, *110* (6), 3479–3500. https://doi.org/https://doi.org/10.1021/cr900339w.
- (35) Qin, J. J.; Li, Y.; Lee, L. S.; Lee, H. Cellulose Acetate Hollow Fiber Ultrafiltration Membranes Made from CA/PVP 360 K/NMP/Water. *J Memb Sci* **2003**, *218* (1–2), 173–183. https://doi.org/10.1016/S0376-7388(03)00170-4.
- (36) Soyekwo, F.; Zhang, Q. G.; Deng, C.; Gong, Y.; Zhu, A. M.; Liu, Q. L. Highly Permeable Cellulose Acetate Nanofibrous Composite Membranes by Freeze-Extraction. *J Memb Sci* **2014**, *454*, 339–345. https://doi.org/10.1016/J.MEMSCI.2013.12.014.
- (37) Mungray, A. A.; Murthy, Z. V. P. Comparative Performance Study of Four Nanofiltration Membranes in the Separation of Mercury and Chromium. *Ionics (Kiel)* **2012**, *18* (8), 811–816. https://doi.org/10.1007/s11581-012-0743-7.
- (38) Henmi, M.; Nakatsuji, K.; Ichikawa, T.; Tomioka, H.; Sakamoto, T.; Yoshio, M.; Kato, T. Self-Organized Liquid-Crystalline Nanostructured Membranes for Water Treatment: Selective Permeation of Ions. *Advanced Materials* **2012**, *24* (17), 2238–2241. https://doi.org/10.1002/adma.201200108.
- (39) Yang, H.; Zhang, Y.; Kato, R.; Rowan, S. J. Preparation of Cellulose Nanofibers from Miscanthus x. Giganteus by Ammonium Persulfate Oxidation. *Carbohydr Polym* **2019**, *212*, 30–39. https://doi.org/10.1016/j.carbpol.2019.02.008.
- (40) Eichhorn, S. J.; Etale, A.; Wang, J.; Berglund, L. A.; Li, Y.; Cai, Y.; Chen, C.; Cranston, E. D.; Johns, M. A.; Fang, Z.; Li, G.; Hu, L.; Khandelwal, M.; Lee, K. Y.; Oksman, K.; Pinitsoontorn, S.; Quero, F.; Sebastian, A.; Titirici, M. M.; Xu, Z.; Vignolini, S.; Frka-Petesic, B. Current International Research into Cellulose as a Functional Nanomaterial for Advanced Applications. *Journal of Materials Science 2022 57:10* 2022, *57* (10), 5697–5767. https://doi.org/10.1007/S10853-022-06903-8.
- (41) Mariano, M.; El Kissi, N.; Dufresne, A. Cellulose Nanocrystals and Related Nanocomposites: Review of Some Properties and Challenges. *J Polym Sci B Polym Phys* **2014**, *52* (12), 791–806. https://doi.org/10.1002/polb.23490.

- (42) Adriana Šturcová, †; Geoffrey R. Davies, ‡ and; Stephen J. Eichhorn*, †. Elastic Modulus and Stress-Transfer Properties of Tunicate Cellulose Whiskers. **2005**. https://doi.org/10.1021/BM049291K.
- (43) Mansouri, J.; Harrisson, S.; Chen, V. Strategies for Controlling Biofouling in Membrane Filtration Systems: Challenges and Opportunities. *J Mater Chem* **2010**, *20* (22), 4567. https://doi.org/10.1039/b926440j.
- (44) Ma, H.; Yoon, K.; Rong, L.; Shokralla, M.; Kopot, A.; Wang, X.; Fang, D.; Hsiao, B. S.; Chu, B. Thin-Film Nanofibrous Composite Ultrafiltration Membranes Based on Polyvinyl Alcohol Barrier Layer Containing Directional Water Channels. *Ind Eng Chem Res* 2010, 49 (23), 11978–11984. https://doi.org/10.1021/ie100545k.
- (45) Smith, E. D.; Hendren, K. D.; Haag, J. V.; Foster, E. J.; Martin, S. M. Functionalized Cellulose Nanocrystal Nanocomposite Membranes with Controlled Interfacial Transport for Improved Reverse Osmosis Performance. *Nanomaterials 2019, Vol. 9, Page 125* 2019, 9 (1), 125. https://doi.org/10.3390/NANO9010125.
- (46) Karim, Z.; Mathew, A. P.; Grahn, M.; Mouzon, J.; Oksman, K. Nanoporous Membranes with Cellulose Nanocrystals as Functional Entity in Chitosan: Removal of Dyes from Water. *Carbohydr Polym* 2014, 112, 668–676. https://doi.org/10.1016/J.CARBPOL.2014.06.048.
- (47) Hore, M. J. A.; Korley, L. S. T. J.; Kumar, S. K. Polymer-Grafted Nanoparticles. *J Appl Phys* **2020**, *128* (3), 30401. https://doi.org/10.1063/5.0019326/1025564.
- (48) Fernandes, N. J.; Koerner, H.; Giannelis, E. P.; Vaia, R. A. Hairy Nanoparticle Assemblies as One-Component Functional Polymer Nanocomposites: Opportunities and Challenges. *MRS Commun* **2013**, *3* (1), 13–29. https://doi.org/10.1557/MRC.2013.9.
- (49) Lettow, J. H.; Yang, H.; Nealey, P. F.; Rowan, S. J. Effect of Graft Molecular Weight and Density on the Mechanical Properties of Polystyrene-Grafted Cellulose Nanocrystal Films. *Macromolecules* **2021**, *54* (22), 10594–10604. https://doi.org/10.1021/ACS.MACROMOL.1C01886.
- (50) Lettow, J. H.; Kaplan, R. Y.; Nealey, P. F.; Rowan, S. J. Enhanced Ion Conductivity through Hydrated, Polyelectrolyte-Grafted Cellulose Nanocrystal Films. *Macromolecules* **2021**, *54* (14), 6925–6936. https://doi.org/10.1021/ACS.MACROMOL.1C01155.
- (51) Kato, R.; Lettow, J. H.; Patel, S. N.; Rowan, S. J. Ion-Conducting Thermoresponsive Films Based on Polymer-Grafted Cellulose Nanocrystals. ACS Appl Mater Interfaces 2020, 12 (48), 54083–54093. https://doi.org/10.1021/acsami.0c16059.
- (52) Macke, N.; Hemmingsen, C. M.; Rowan, S. J. The Effect of Polymer Grafting on the Mechanical Properties of PEG-Grafted Cellulose Nanocrystals in Poly(Lactic Acid). *Journal of Polymer Science* 2022, 60 (24), 3318–3330. https://doi.org/10.1002/POL.20220127.

- (53) Araki, J.; Wada, M.; Kuga, S. Steric Stabilization of a Cellulose Microcrystal Suspension by Poly(Ethylene Glycol) Grafting. *Langmuir* **2001**, *17* (1), 21–27. https://doi.org/10.1021/la001070m.
- (54) Halperin, A.; Tirrell, M.; Lodge, T. P. Tethered Chains in Polymer Microstructures. In *Advances in Polymer Science*; 1992; Vol. 100, pp 31–71. https://doi.org/10.1007/BFb0051635.
- (55) Kaiser, E.; Colescott, R. L.; Bossinger, C. D.; Cook, P. I. Color Test for Detection of Free Terminal Amino Groups in the Solid-Phase Synthesis of Peptides. *Anal Biochem* **1970**, *34* (2), 595–598. https://doi.org/10.1016/0003-2697(70)90146-6.
- (56) Dan, N.; Tirrell, M. Polymers Tethered to Curved Interfaces. A Self-Consistent-Field Analysis. *Macromolecules* **1992**, 25 (11), 2890–2895. https://doi.org/10.1021/MA00037A016/.
- (57) Jiao, Y.; Tibbits, A.; Gillman, A.; Hsiao, M. S.; Buskohl, P.; Drummy, L. F.; Vaia, R. A. Deformation Behavior of Polystyrene-Grafted Nanoparticle Assemblies with Low Grafting Density. *Macromolecules* 2018, 51 (18), 7257–7265. https://doi.org/10.1021/acs.macromol.8b01524.
- (58) Lenart, W. R.; Hore, M. J. A. Structure–Property Relationships of Polymer-Grafted Nanospheres for Designing Advanced Nanocomposites. *Nano-Structures & Nano-Objects* **2018**, *16*, 428–440. https://doi.org/10.1016/J.NANOSO.2017.11.005.
- (59) Fischer, S.; Salcher, A.; Kornowski, A.; Weller, H.; Förster, S. Completely Miscible Nanocomposites. *Angewandte Chemie International Edition* **2011**, *50* (34), 7811–7814. https://doi.org/10.1002/ANIE.201006746.
- (60) Ohno, K.; Morinaga, T.; Takeno, S.; Tsujii, Y.; Fukuda, T. Suspensions of Silica Particles Grafted with Concentrated Polymer Brush: Effects of Graft Chain Length on Brush Layer Thickness and Colloidal Crystallization. *Macromolecules* **2007**, *40* (25), 9143–9150. https://doi.org/10.1021/ma071770z.
- (61) Morinaga, T.; Honma, S.; Ishizuka, T.; Kamijo, T.; Sato, T.; Tsujii, Y. Synthesis of Monodisperse Silica Particles Grafted with Concentrated Ionic Liquid-Type Polymer Brushes by Surface-Initiated Atom Transfer Radical Polymerization for Use as a Solid State Polymer Electrolyte. *Polymers (Basel)* 2016, 8 (4). https://doi.org/10.3390/POLYM8040146.
- (62) Ohno, K.; Morinaga, T.; Koh, K.; Tsujii, Y.; Fukuda, T. Synthesis of Monodisperse Silica Particles Coated with Well-Defined, High-Density Polymer Brushes by Surface-Initiated Atom Transfer Radical Polymerization. *Macromolecules* **2005**, *38* (6), 2137–2142. https://doi.org/10.1021/MA048011Q.
- (63) Hansoge, N. K.; Keten, S. Effect of Polymer Chemistry on Chain Conformations in Hairy Nanoparticle Assemblies. *ACS Macro Lett* **2019**, 8 (10), 1209–1215. https://doi.org/10.1021/acsmacrolett.9b00526.

- (64) See Toh, Y. H.; Loh, X. X.; Li, K.; Bismarck, A.; Livingston, A. G. In Search of a Standard Method for the Characterisation of Organic Solvent Nanofiltration Membranes. *J Memb Sci* **2007**, *291* (1–2), 120–125. https://doi.org/10.1016/J.MEMSCI.2006.12.053.
- (65) Microdyn Nadir Membrane Filters, UC500, RC, UF, 25mm, 5/pk 1121. https://www.sterlitech.com/microdyn-nadir-membrane-filters-uc500-rc-uf-25mm-5-pk.html (accessed 2024-01-08).
- (66) Novellani, M.; Santini, R.; Tadrist, L. Experimental Study of the Porosity of Loose Stacks of Stiff Cylindrical Fibres: Influence of the Aspect Ratio of Fibres. *European Physical Journal B* **2000**, *13* (3), 571–578. https://doi.org/10.1007/S100510050069/.
- (67) Wenli Zhang. Experimental and Computational Analysis of Random Cylinder Packings with Applications. *LSU Doctoral Dissertations* **2006**, 163.
- (68) Wang, X.; Zhang, D.; Wu, J.; Protsak, I.; Mao, S.; Ma, C.; Ma, M.; Zhong, M.; Tan, J.; Yang, J. Novel Salt-Responsive SiO2@Cellulose Membranes Promote Continuous Gradient and Adjustable Transport Efficiency. *ACS Appl Mater Interfaces* **2020**, *12* (37), 42169–42178. https://doi.org/10.1021/ACSAMI.0C12399.
- (69) Drobek, T.; Spencer, N. D.; Heuberger, M. Compressing PEG Brushes. *Macromolecules* **2005**, *38* (12), 5254–5259. https://doi.org/10.1021/MA0504217.
- (70) Shi, L.; Zhang, J.; Zhao, M.; Tang, S.; Cheng, X.; Zhang, W.; Li, W.; Liu, X.; Peng, H.; Wang, Q. Effects of Polyethylene Glycol on the Surface of Nanoparticles for Targeted Drug Delivery. *Nanoscale* **2021**, *13* (24), 10748–10764. https://doi.org/10.1039/D1NR02065J.
- (71) Liu, M.; Yu, C.; Dong, Z.; Jiang, P.; Lü, Z.; Yu, S.; Gao, C. Improved Separation Performance and Durability of Polyamide Reverse Osmosis Membrane in Tertiary Treatment of Textile Effluent through Grafting Monomethoxy-Poly(Ethylene Glycol) Brushes. Sep Purif Technol 2019, 209, 443–451. https://doi.org/10.1016/J.SEPPUR.2018.07.072.
- (72) Rajendran, S. R. C. K.; Mason, B.; Doucette, A. A. Review of Membrane Separation Models and Technologies: Processing Complex Food-Based Biomolecular Fractions. *Food Bioproc Tech* **2021**, *14* (3), 415–428. https://doi.org/10.1007/S11947-020-02559-X/.

For Table of Contents Only:

